Biochimica et Biophysica Acta 1828 (2013) 1347–1356

Contents lists available at SciVerse ScienceDirect

Biochimica et Biophysica Acta

journal homepage: www.elsevier.com/locate/bbamem

Biophysical changes induced by xenon on phospholipid bilayers

Ryan D. Booker, Amadeu K. Sum *

Department of Chemical and Biological Engineering, Colorado School of Mines, 1600 Illinois Street, Golden, CO 80401, USA

ARTICLE INFO

Article history:
Received 3 August 2012
Received in revised form 28 December 2012
Accepted 22 January 2013
Available online 30 January 2013

Keywords:
General anesthesia
Lipid membrane
Phase transition
Simulation
Molecular dynamics

ABSTRACT

Structural and dynamic changes in cell membrane properties induced by xenon, a volatile anesthetic molecule, may affect the function of membrane-mediated proteins, providing a hypothesis for the mechanism of general anesthetic action. Here, we use molecular dynamics simulation and differential scanning calorimetry to examine the biophysical and thermodynamic effects of xenon on model lipid membranes. Our results indicate that xenon atoms preferentially localize in the hydrophobic core of the lipid bilayer, inducing substantial increases in the area per lipid and bilayer thickness. Xenon depresses the membrane gel–liquid crystalline phase transition temperature, increasing membrane fluidity and lipid head group spacing, while inducing net local ordering effects in a small region of the lipid carbon tails and modulating the bilayer lateral pressure profile. Our results are consistent with a role for nonspecific, lipid bilayer-mediated mechanisms in producing xenon's general anesthetic action.

1. Introduction

General anesthesia is a physiological state characterized by loss of consciousness, loss of sensation through analgesic effects, immobilization, and temporary amnesia [1]. The physiological effects are known to be produced through depression of nerve function but, despite the fact that general anesthesia has been accepted for clinical use for over a century and is administered to approximately 21 million patients annually in the United States alone [2], the specific molecular mechanisms by which anesthetic agents induce an anesthetic state remain poorly understood.

The correlation between anesthetic efficacy and lipid solubility, known as the Meyer–Overton correlation [3,4], led the majority of research on the molecular mechanisms of general anesthetics to be focused on the interactions between anesthetic agents and the lipid bilayers of neuronal membranes for over 80 years. More recently, however, a number of researchers, most notably Franks and Lieb [5], have shifted the focus to direct protein interactions. Much research, outlined extensively by Barash et al. [6], Urban [7,1], and Franks [8], has focused on a mechanism involving direct interactions with hydrophobic pockets or clefts in transmembrane ion channels and protein targets of general anesthetic agents are well supported by the evidence. However, while significant progress has been made in characterizing the interactions between anesthetics and individual protein and central nervous system (CNS) targets, these investigations have not identified an individual target or comprehensive mechanism of action capable of mediating the complete anesthetic effect [9]. Indeed, it increasingly appears that the clinical effects of general anesthesia are the result of multiple molecular mechanisms occurring at different targets.

Of particular interest recently, both for its lack of undesirable side effects in clinical settings and for its unique molecular interactions, is the noble gas xenon. The clinical viability of xenon as an anesthetic agent has been known for over 60 years [10]. However, its clinical use has been largely curtailed by its high cost until recently [11]. During the last decade, the desire to replace or supplement the use of nitrous oxide due to its environmental impacts [12] and the advantageous pharmacokinetic profile [13], neuroprotective properties [14,15], and potent analgesic effects [16] of xenon have led to renewed interest in xenon in clinical settings [11,17,18].

However, xenon's simple, spherical shape and the fact that it is essentially inert pose an interesting conundrum in regard to the mechanisms of its anesthetic action. Xenon appears to have no significant effect on the most commonly implicated anesthetic target, $GABA_A$ receptors [19–21]. Xenon has been shown to act on glutamatergic receptors, with inhibition of NMDA receptors being the mechanism implicated most often [19,22,20,23,24]. Using molecular dynamics, Liu et al. [25] identify several potential action sites of xenon in the ligand-binding domain of an NMDA receptor. However, results with glutamatergic receptors have been somewhat inconsistent, with other researchers showing that xenon acts on non-NMDA glutamatergic receptors in *Caenorhabditis elegans* [26], although it is possible that general anesthesia occurs by different mechanisms in *C. elegans* versus humans and other mammals. Furthermore, recent research has indicated that NMDA receptors do not mediate the immobilizing effects of xenon and other inhaled anesthetics [27], although this does not preclude the possibility that NMDA receptors mediate the other effects of general anesthesia. It has also been shown that one minimum alveolar concentration (MAC) of xenon

* Corresponding author. Tel.: +1 303 273 3873; fax: +1 303 273 3730.
E-mail address: asum@mines.edu (A.K. Sum).

0005-2736/$ – see front matter © 2013 Elsevier B.V. All rights reserved.
http://dx.doi.org/10.1016/j.bbamem.2013.01.016

actually depresses metabolic activity in the human brain [28,29], whereas two anesthetics that have also been shown to inhibit NMDA receptors, ketamine and nitrous oxide, increase cerebral metabolism [27]. This inconsistency with anesthetic agents known to interact with NMDA receptors may indicate that glutamatergic receptors play little or no role in the anesthetic effects of xenon in vivo [28]. Xenon has also been shown to exert effects on nicotinic acetylcholine receptors [22] and certain potassium channels [30], some of which have recently been implicated as playing a role in the anesthetic effect [31,32], but the significance of these results remains unclear.

Recently, there has been substantial renewed interest in the role lipid bilayers play in modulating the function of membrane proteins [33–36]. It has been shown that the open probability of voltage-dependent potassium channels is affected by the mechanical state of the surrounding lipid membrane [37] and that small changes in bilayer thickness can reverse the response polarity of gramicidin A channels [38]. Furthermore, amphiphiles have been shown to regulate voltage-gated ion channel function through a lipid bilayer-mediated mechanism [39,40] and $GABA_A$ receptor function is regulated by lipid bilayer elasticity [41]. Cantor [42] proposed that an inhomogeneous modulation of the lateral pressure (more accurately called the stress virial) profiles in the cellular membrane by anesthetic molecules exerts lateral forces on transmembrane gated ion channels, inducing effects on channel current by increasing the energy needed to change the channel between open and closed conformations. Other recent studies have since shown that a change in the lateral pressure profile could influence the conformation of ion channels [43,44] and molecular dynamics simulations with ethanol and 1-alkanols have indicated that this mechanism is consistent with the action of general anesthetics [45,46]. Furthermore, this hypothesis predicts the alkanol cutoff effect and anomalously low anesthetic potencies of strongly hydrophobic molecules such as perfluorocarbons.

It is generally accepted that cellular membranes in vivo can be described by a fluid mosaic model, proposed by Singer and Nicolson [50], in which proteins are embedded within a lipid bilayer and all components can diffuse laterally within the plane of the membrane [51]. The accumulation of a variety of small molecules in a lipid bilayer is known to cause changes in the bilayer biophysical and thermodynamic properties and these interactions between small molecules and lipid bilayers have commonly been studied through computer simulation. Molecular dynamics studies have primarily focused on small hydrocarbons and organic acids [52–55], sugars [56–59], alcohols [60,54,61,45,62], and some small biological molecules [63,64].

Molecular dynamics studies of interactions between general anesthetic agents and lipid membranes have been more limited in scope. Older simulations were generally restricted to coarse-grained simulations [65], short timescales [60,66–68] or studies solely of alcohols [60,61,45]. However, more recently, a number of atomistic simulation studies conducted over longer timescales have indicated substantial effects of anesthetic agents on a number of lipid bilayer properties. Stimson et al. [69] performed 100 ns, atomistic molecular dynamics simulations investigating the interactions between xenon and dioleoylphosphatidylcholine (DOPC) bilayers, with initial results indicating that partitioning of xenon into the bilayer causes small increases in the area per lipid and orientational order of the lipid acyl chains. More recently, Yamamoto et al. [70] reported an MD study of POPE bilayer exposed to xenon at different pressures to probe the pressure reversal effect in general anesthesia. The results from their simulations showed that pressure had little effect on the properties of the lipid bilayer, but suggested that xenon accumulated in the middle of the lipid bilayer and had its diffusivity substantially decreased. Simulation studies conducted by Tu et al. [71], studying halothane, and Darvas et al. [72], studying halothane, chloroform, diethyl ether, and enflurane, show reversal of the effects of general anesthetic agents on membrane properties at high pressures.

Here, we investigate the interactions of xenon with model phospholipid membranes using molecular dynamics (MD) simulations of pure DOPC bilayers in two initial configurations with xenon at a range of concentrations and pressures and over timescales of 150–300 ns. Differential scanning calorimetry (DSC) measurements are presented to characterize the effects of xenon on lipid membrane phase transition temperatures and fluidity. Xenon is shown to exert broad biophysical effects on membrane fluidity, lateral pressure profiles near the lipid head groups, and bilayer structure. These interactions are consistent with a lipid bilayer-mediated mechanism of general anesthetic action.

2. Materials and methods

2.1. Molecular dynamics simulations

Molecular dynamics simulations were performed on two different types of systems: 1) single bilayer systems containing 288 DOPC molecules arranged in a bilayer structure (144 molecules in each leaflet); and 2) double bilayer systems containing 576 DOPC molecules arranged in two bilayers, separated by aqueous phases. A DOPC molecule was initially constructed and then arranged in a bilayer configuration (Fig. S1 in the Supporting material is a line diagram of a DOPC molecule). A total of six xenon concentrations were simulated: 0, 1, 1.5, 2, 2.5, and 3 xenon atoms per lipid. The minimum alveolar concentration (MAC) for xenon is 71% [73]. Stimson et al. [69] point out that the specific concentration, in a tissue comparable to those simulated here, required to induce an anesthetic state is unknown and this remains true. The concentrations chosen here are comparable to those used in previous studies [69,70].

Bilayers were fully hydrated, with 40 water molecules per lipid in the systems containing xenon concentrations of 0 to 2 xenon atoms per lipid and 50 water molecules per lipid in the systems containing 2.5 and 3 xenon atoms per lipid. Prior to insertion of xenon atoms, the bilayers were heated to 450 K to erase memory effects from the initial configuration. Bilayers were then allowed to equilibrate for 20 ns at 310 K. Initial configurations were generated by adding a number of excess water molecules equal to the intended number of xenon atoms, then randomly replacing the appropriate number of water molecules with xenon atoms. Fig. 1 shows snapshots of the initial (A) and final (B) configurations of a double bilayer system. Fig. 3B shows a snapshot of a single bilayer system and Fig. S3 shows snapshots of the initial (A) and final (B) configurations of a single bilayer system. For the results below, data were analyzed over the last 20 ns for single bilayer simulations and over the last 40 ns for double bilayer systems, when the systems had reached dynamic equilibrium. The systems reached dynamic equilibrium when net diffusion of xenon between the bilayer and aqueous phases ceased and when changes in bilayer surface area over time stabilized around a mean value (this was true over the final 20 ns for all single bilayer systems and over the final 40 ns for all double bilayer systems). An example of the distribution of xenon between the aqueous phase and lipid bilayer in a double bilayer is shown in Fig. S4.

The forcefield employed for the lipids used the Berger lipid parameters [74] with the GROMOS forcefield. Water was represented by the single point charge (SPC) model [75] and the xenon atoms were represented as simple Lennard–Jones sites with $\varepsilon = 1.837$ kJ/mol and $\sigma = 0.410$ nm [76]. This approach is consistent with previous MD simulations of lipid bilayers and with simulations of bilayers with xenon specifically [69,70]. Simulations were performed using single precision GROMACS 4 [77] with the Berendsen thermostat and barostat [78]. Simulations were held at a constant temperature of 310 K, above the $L_{\beta\alpha}$ (gel–liquid crystalline) phase transition temperature for DOPC (−20 °C [79]), and four different pressures were used: 1, 50, 100, and 200 bar. Anisotropic pressure coupling was applied. A short range cut-off of 1.0 nm was used for nonbonded interactions (Coulombic and Lennard-Jones) and long-range electrostatic interactions were calculated by the particle-mesh Ewald method

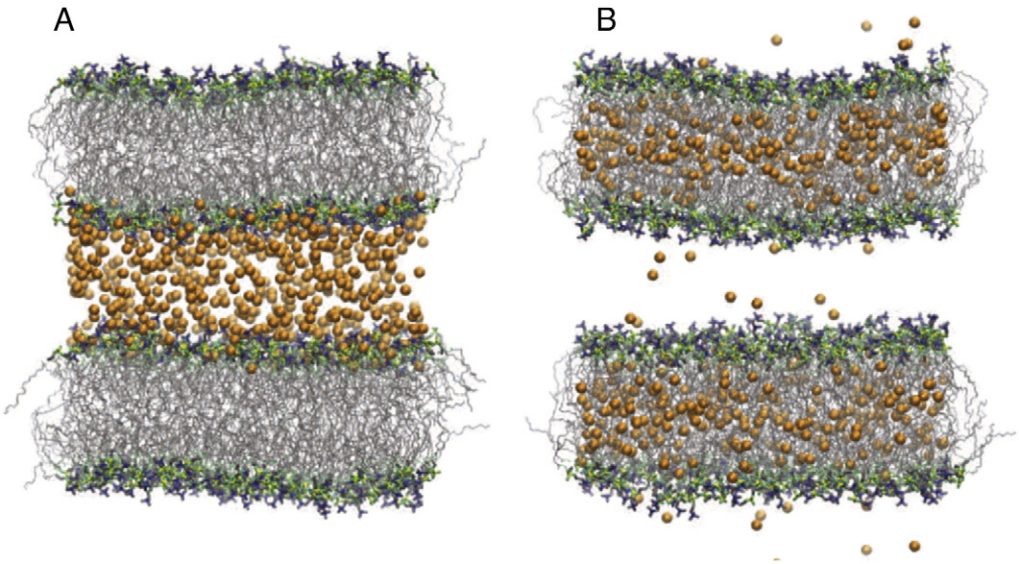

Fig. 1. Illustration of a double DOPC bilayer system in the MD simulations. (A) Initial configuration with xenon in the aqueous phase. (B) Final configuration with xenon at equilibrium partitioning between bilayer and aqueous phases. Carbon (*gray*), oxygen (*green*), nitrogen (*blue*), and phosphorous (*yellow*) in head groups are shown using a licorice representation while the lipid tails are shown as lines. Xenon is represented by orange spheres. Water molecules are not shown for clarity.

[80,81]. A time-step of 2 fs was used for all simulations and the LINCS algorithm was used to apply bond constraints [82]. Periodic boundary conditions were applied in all directions.

2.2. Liposome preparation

In order to further investigate the effects of xenon on membrane fluidity and correlate these results to the simulation studies, model cell membranes consisting of dielaidoylphosphatidylcholine (DEPC) liposomes (large multilamellar vesicles) were prepared (Fig. S2 in the Supporting material is a line diagram of a DEPC molecule). DEPC undergoes an $L_{\beta\alpha}$ (gel–liquid crystalline) phase transition at 12 °C [79]. DEPC [18:1 Δ9-*trans* phosphocholine] was obtained from Avanti Polar Lipids (Alabaster, AL) in powder form. Liposomes (multilamellar vesicles) were prepared by dissolving 20 mg/mL of powdered lipids into deionized water. Lipids were vigorously mixed for 1 h and the liposomes were then allowed to age overnight at approximately 20 °C. After aging, the large multilamellar vesicles were stored at approximately 20 °C (above the DEPC phase transition temperature) and used within 48 h.

2.3. Differential scanning calorimetry

To determine the effects of xenon on membrane fluidity, the $L_{\beta\alpha}$ (gel–liquid crystalline) phase transition temperature was determined at xenon pressures of 3 and 10 bar using a high-pressure microdifferential scanning calorimeter (μ-DSC VIIa, Setaram Inc.). DEPC was used for these experiments due to its higher phase transition temperature than the simulated lipid, DOPC. Samples of 25–30 mg were placed in a Hastelloy C276 cell with a fixed internal volume of 0.5 mL. The sample cell and a reference cell were connected to a xenon cylinder (99.999% pure from Matheson Tri-Gas) through a custom-designed high-pressure panel. Heating and cooling of the cells were achieved using Peltier heating elements.

The procedure for the DSC measurements was as follows. Samples were pressurized to the selected xenon pressure at 30 °C. The temperature was then ramped to −2 °C at 1 °C/min and held at −2 °C for 10 min. The temperature was then ramped back to 30 °C, with a heating rate of 0.3 °C/min. Heating and cooling cycles were repeated, with one measurement of T_m per cycle, until equilibrium, as indicated by a lack of change in the phase transition temperature, was reached. T_m was measured during heating cycles ($L_{\beta\alpha}$ phase transition) and the liposome phase transition region was thus indicated by an endothermic heat flow peak. The phase transition temperature was determined as the minimum of the endothermic heat flow peak.

3. Results

3.1. Xenon partitioning and effects on lipid tail ordering

At dynamical equilibrium, approximately 97% of the xenon atoms localize within the bilayer. Fig. 1B shows an example of the final configuration of a double bilayer system in which xenon has permeated into the membrane, leaving approximately 3% of the xenon atoms in the bulk aqueous phase. Neither the xenon concentration in the system nor the system pressure substantially affects the xenon partitioning between the aqueous phase and bilayer at equilibrium (see the Supporting material for a discussion on the dynamics of xenon permeation into the bilayers). The GROMOS forcefield utilized here does not incorporate the polarizability of xenon, which is important to its behavior, particularly in aqueous systems. Xenon's high polarizability (4) compared to the other noble gases increases its affinity for hydrophobic environments. It is thus interesting to note the substantial partitioning of the xenon into the hydrophobic core of the bilayer despite the lack of polarizability in the forcefield.

The partitioning of the xenon atoms within the lipid bilayer systems can be more quantitatively assessed by examining the partial densities of the systems at equilibrium (see Fig. S5 in the Supporting material for the component densities for water, DOPC, the phosphorous atoms of the DOPC head groups, and xenon at three concentrations). For this work, the interior of the bilayer is defined as the region between the phosphorus atoms in the lipid head groups of the two bilayer leaflets (see Fig. S5 in the Supporting material). Xenon is found to preferentially localize in the hydrophobic core of the bilayer, below the lipid head groups. The region of highest xenon density occurs between the *cis* double bonds and the terminal carbon atoms in the lipid acyl chains, although a substantial amount of xenon does localize in the gap region between the terminal carbons. This localization of xenon within the hydrophobic core of the lipid bilayer was also found in previous simulation studies by Stimson et al. [69] and Yamamoto et al. [70].

The localization of xenon in the hydrophobic core of the bilayer has substantial implications for the ordering of the lipid acyl chains. Fig. 2B shows the lipid tail deuterium order parameters at each of the six xenon concentrations that were simulated. The order parameter [83] provides a quantitative measure of the alignment of the lipid tails. Increasing xenon concentration causes a corresponding increase in the ordering of the lipid tails, primarily between the *cis* double bonds of the acyl tails and the terminal carbons, in the regions corresponding to the highest xenon density. The increase in the order parameters indicates a more ordered and constrained environment for the acyl chains, resulting in a relative decrease in membrane fluidity from the *cis* double bonds to the terminal carbons.

3.2. Effects of xenon on membrane structure

Fig. 3A shows the relationship between area per lipid and increasing xenon concentration. The area per lipid is defined as the area of the *xy*-plane of the simulation box divided by the number of lipids per leaflet, as shown in Fig. 3B. Again, pressure does not substantially affect the bilayer surface area because the bilayers are essentially incompressible. The value for the area per lipid at 1 bar for a pure DOPC bilayer (no xenon) agrees closely with previous results obtained by Alwarawrah et al. [84], differing by 3.1% or 0.02 nm^2. The trend of increasing bilayer surface area with increasing xenon concentration is also reported by Stimson et al. [69] and Yamamoto et al. [70]. The observed simultaneous increase in the area per lipid and in the ordering of the acyl chains (comparison between Figs. 2B and 3A) with increasing xenon concentration is a counterintuitive trend. In general, increased bilayer surface area is accompanied by decreased acyl chain ordering, resulting in increased membrane fluidity. The constraining of the lipid tails indicative of increased order parameter corresponds to increased lipid packing and thus decreased bilayer surface area. This apparent inconsistency appears to be the result of two competing effects when xenon is present in the lipid bilayer, which are elucidated by the differential scanning calorimetry results and will be discussed later in the paper.

Localization of xenon within the lipid membrane also causes an increase in bilayer thickness, shown in Fig. 3C (this is also observed as an increase in the distance between the peaks in Fig. S5 in the Supporting material). In Fig. 3D, the total area of the bars indicates the change in bilayer thickness at each xenon concentration from the thickness when no xenon is present, while the smaller, darkly shaded areas represent the portion of the total change in thickness accounted for by an increase in the gap between the terminal carbons of the two bilayer leaflets. The bilayer thickness increases substantially with increasing xenon concentration, with an increase of approximately 0.45 nm observed from no xenon to 3 xenon per lipid. As shown in Fig. 3D, an increase in the gap between the terminal carbons accounts for 75–85% of the total increase in bilayer thickness. The remaining increase in bilayer thickness is likely caused by the straightening of the lipid acyl chains due to increased order parameter. While no pressure effects were observed for the lipid tail order parameters or bilayer surface area, at the highest pressure (200 bar) and high xenon concentration (2.5–3.0 xenon per lipid), there is a small increase in bilayer thickness. This increase in thickness is entirely accounted for by an increase in the gap between the terminal carbons, thus explaining the increase in thickness without a statistically significant corresponding decrease in bilayer surface area.

Thus, the accumulation of xenon in the membrane induces membrane swelling through increases in both bilayer thickness and surface area. This swelling is accompanied by a decrease in lipid occupied volume within the membrane, which is evident from a decrease in the DOPC density within the core of the bilayer with increasing xenon concentration (see Fig. S6 in the Supporting material).

3.3. Effects of xenon on lipid phase transition and fluidity

In order to determine the effects of the accumulation of xenon on the main ($L_{\beta\alpha}$, gel to liquid crystalline) phase transition temperature (T_m) and fluidity of lipid membranes, we conducted a series of DSC measurements on large multilamellar vesicles (LMVs) in the presence of xenon gas. Dielaidoylphosphatidylcholine [DEPC, 18:1 Δ9-*trans* phosphocholine] was used in these measurements, rather than DOPC [18:1 Δ9-*cis* phosphocholine] used in the molecular dynamics simulations, due to its higher phase transition temperature. Pure DOPC liposomes undergo a phase transition at approximately −20 °C [79], which is low enough below the freezing point of water that it is very difficult to prevent freezing of water during the cooling stage in the DSC measurements. DEPC, however, undergoes an $L_{\beta\alpha}$ phase transition at approximately 12 °C [79], allowing DSC scans above the freezing point of water, resulting in clean and clear scans of the phase transition heat flow.

The $L_{\beta\alpha}$ phase transition temperature for the pure DEPC liposomes, measured prior to charging with xenon, was found to be 11.8 ± 0.4 °C, within experimental error of the accepted value of 12 °C [79]. Fig. 4A

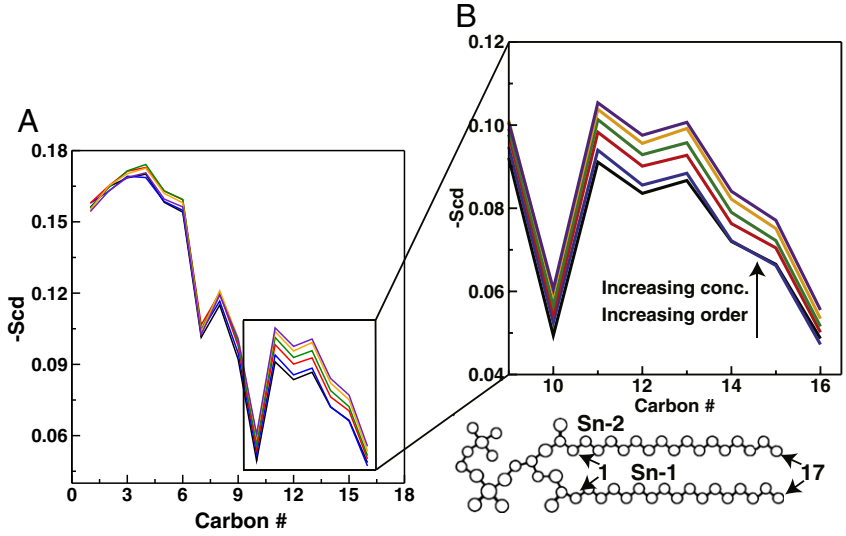

Fig. 2. Structural changes to bilayer induced by xenon. (A) Acyl chain deuterium order parameter for Sn-1 tail. (B) Expanded view of acyl chain deuterium order parameter for region including and after *cis* double bond in Sn-1 tail. The Sn-2 tail, not shown, produces the same results as the Sn-1 tail. Coloring of lines corresponds to 0 (*black*), 1 (*blue*), 1.5 (*red*), 2 (*green*), 2.5 (*orange*), and 3 (*purple*) xenon per lipid.

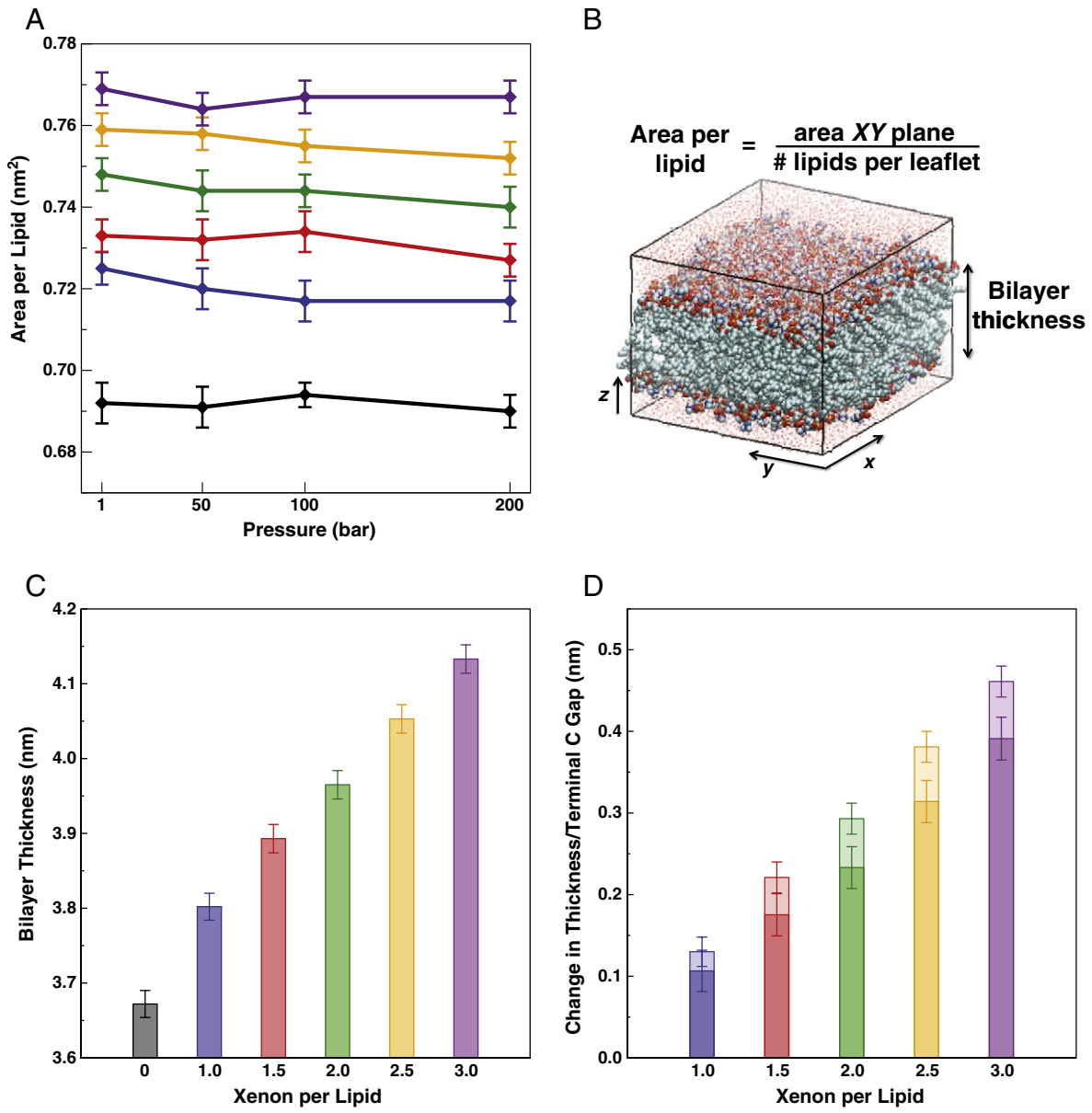

Fig. 3. Effect of xenon on bilayer structural properties. (A) Area per lipid for each of the six xenon concentrations and four pressures. (B) Representation of single bilayer with definitions of coordinate system, area per lipid, and bilayer thickness. (C) Bilayer thickness for each of the six xenon concentrations. (D) Change in bilayer thickness (full bars) from thickness at 0 xenon per lipid and change in gap between terminal carbons (dark shading) from terminal carbon gap at 0 xenon per lipid for 1–3 xenon per lipid. Coloring of lines/bars corresponds to 0 (*black*), 1 (*blue*), 1.5 (*red*), 2 (*green*), 2.5 (*orange*), and 3 (*purple*) xenon per lipid. Error bars based on standard deviation.

shows the change in liposome phase transition temperature with increasing time for DEPC liposomes exposed to xenon gas at 10 bar. Each peak represents the heat flow curve from a different temperature cycle, with each cycle occurring approximately 2.6 h apart. The $L_{\beta\alpha}$ phase transition temperature decreased substantially during the first cycle, dropping to approximately 5.5 °C, followed by a steady decrease in T_m until an equilibrium value of 4.8 ± 0.4 °C was reached. Thus, the $L_{\beta\alpha}$ phase transition temperature for DEPC liposomes decreases 7.0 °C when at equilibrium with xenon at 10 bar.

Xenon is also a clathrate hydrate former and under the conditions of this study, these crystalline structures are easily formed. After reaching an equilibrium concentration of xenon in the bilayer, xenon clathrate hydrate formation was induced in the liposome–xenon system by a further temperature decrease to −10.0 °C. Formation of xenon hydrates in the liposome solution was evident from exothermic and endothermic heat flow peaks, representing hydrate formation and dissociation, respectively, in a similar manner to that described in [85] (see Fig. S7 in the Supporting material for hydrate dissociation curves). In the presence of xenon hydrates, the DEPC liposomes T_m shifted to 9.2 ± 0.4 °C (see Fig. 4B) for xenon charged to 10 bar. Similar results were found when xenon was charged to 13 bar and 17 bar. The similar transition temperatures found for the three different pressures in the presence of clathrate hydrate is likely due to the increased formation of xenon hydrate at higher pressures, leaving similar amounts of xenon available for permeation into the liposomes at the three pressures. This is the first instance that the thermodynamics of these liposome–xenon clathrate hydrate systems have been measured. The increase in the $L_{\beta\alpha}$ phase transition temperature when xenon clathrate hydrate is formed versus when it is not suggests that the change in liposome T_m induced by xenon is concentration dependent. As the clathrate hydrate is formed, a significant amount of xenon is enclathrated in the crystalline structure, not only reducing the available concentration of xenon for permeation into the liposomes, but also removing xenon from the liposomes. This apparent concentration dependence was further explored by repeating the T_m

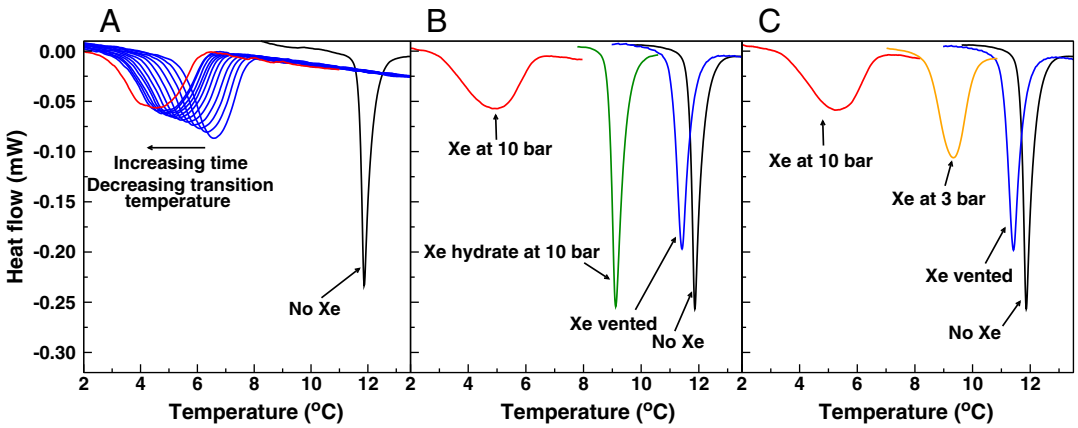

Fig. 4. Thermograms of DEPC liposome $L_{\beta\alpha}$ phase transition temperatures in the presence of xenon. (A) Change in phase transition temperature over time for liposome exposed to xenon at 10 bar. Each heat flow peak represents a different cycle. Cycle length was 2.6 h. (B) Phase transitions for liposome under different conditions corresponding to xenon at 10 bar, xenon hydrates formed at 10 bar, and vented xenon. (C) Pressure (concentration) dependence of phase transitions for liposome. The phase transition after venting xenon was identical for the 3 and 10 bar conditions.

measurements with xenon gas at 3 bar, rather than at 10 bar. At equilibrium with xenon at 3 bar, the DEPC liposomes' T_m was found to be 9.3 ± 0.4 °C, a decrease of only 2.5 °C from the pure DEPC liposomes T_m. Thus, it is clear that the effect of xenon on the $L_{\beta\alpha}$ phase transition temperature of liposomes is concentration dependent. The values for T_m are summarized in Table 1.

4. Modulation of membrane lateral pressure profile

Cantor [42] proposed that an inhomogeneous modulation of the lateral pressure profiles in the cellular membrane by anesthetic molecules changes the lateral forces exerted on transmembrane gated ion channels, inducing effects on channel current by increasing the energy needed to change the channel between open and closed conformations. Fig. 5 shows the lateral pressure profile for a DOPC bilayer with xenon at several concentrations and details the associated changes induced by xenon on the properties of the bilayers.

Substantial lateral pressure, particularly in the region approximately 1.5 to 2.5 nm from the bilayer center (near the lipid head groups), is observed. The positive peak at the membrane–water interface (~±2.6 nm) is generally interpreted as being due to repulsion due to electrostatic and steric interactions, as well as a hydration repulsion component [45]. Unlike the findings for ethanol [45], this peak appears to be largely unchanged by the accumulation of xenon in the bilayer. Closer to the bilayer center (~±1.5–2.0 nm), there is a region characterized by substantial negative pressure, indicating an attractive contribution due to interfacial energy between water and the hydrophobic core of the bilayer. Unlike in previous simulation studies, this negative peak is found to be bimodal. This bimodal response may originate from additional interactions at the region between the lipid head groups and hydrophobic core being captured. As with the results of Terama et al. [45] for ethanol, the magnitude of this peak is reduced by approximately 100 to 200 bar by the presence of xenon. This reduction is increased at higher xenon concentrations (2.5 and 3 xenon per lipid) but that data are not shown because the expansion of the bilayer makes comparison with the other lateral pressure profiles difficult. This decrease in the magnitude of the negative peak is likely caused by a decrease in surface tension between water and the hydrophobic core of the bilayer due to the presence of xenon at and near this interface.

There is substantial modulation of the lateral pressure profile near the regions where xenon primarily localizes at equilibrium (the

Table 1
Gel–liquid crystalline ($L_{\beta\alpha}$) phase transition temperatures and phase transition range for DEPC liposomes obtained from DSC measurements[a].

Sample	T_m (°C)[b]	T_{lower} (°C)[c]	T_{upper} (°C)[c]	Range (°C)
No xenon	11.8	11.7	12.2	0.5
Xe at 3 bar (no hydrate)	9.3	8.5	10.1	1.6
Xe at 10 bar (no hydrate)	4.8	3.3	6.4	3.1
Xe at 10 bar (with hydrate)	9.2	8.9	9.6	0.7
Xe at 13 bar (with hydrate)	9.2	8.9	9.6	0.7
Xe at 17 bar (with hydrate)	9.4	8.8	10.0	1.2
Xenon vented	11.4	11.0	11.8	0.8

[a] Error (based on SD) in temperature measurements is ±0.4 °C.
[b] The value for the phase transition temperature (T_m) is the minimum of the heat flow.
[c] The lower (T_{lower}) and upper (T_{upper}) phase transition temperatures are taken as the onset and return, respectively, of heat flow deviation from the baseline.

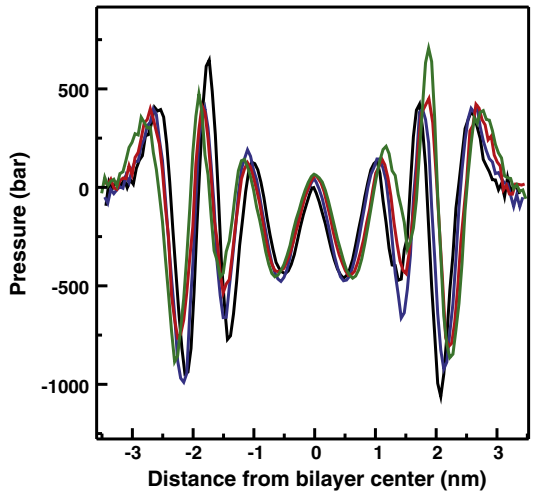

Fig. 5. The lateral pressure profile for a DOPC bilayer at 1 bar and 310 K with xenon at several concentrations. The higher xenon concentrations (2.5 and 3 xenon per lipid) are not shown due to the large change in bilayer thickness. To calculate the lateral pressure profiles, the trajectories from the 150 ns single bilayer simulation runs were analyzed using the 3D pressure field method developed by Ollila et al. [86]. The final 30 ns of the simulation runs were used in the analysis. This method involves the calculation of the lateral pressure profile from the Irving–Kirkwood contour [87] by discretizing the local pressure into small cubes, allowing for calculation of the average pressure over arbitrary volume elements. Coloring of lines corresponds to xenon concentrations of 0.0 (black), 1.0 (blue), 1.5 (red), and 2.0 (green) xenon per lipid.

hydrophobic core of the bilayer). Unlike ethanol, which localizes much nearer the lipid head groups, no reduction in the positive peak at the membrane–water interface is observed because the low concentrations of xenon near the lipid head groups are unable to screen electrostatic interactions between the head groups as the higher concentrations of ethanol do. While modulation of the lateral pressure profile as a mechanism for general anesthesia is theoretically consistent with current understanding of the general anesthetic effect, the specific effects of lateral pressure on transmembrane proteins are unclear and significant experimental and simulation work will be needed to further elucidate this effect. It has been hypothesized that the shape of some ion channels may be influenced by changes in surrounding membrane properties or that changes in membrane properties may influence the energy required for a transmembrane ion channel to undergo a conformational change [34,36], but the implications for xenon's anesthetic effect remain conjecture. However, if modulation of the lateral pressure profile does play a role in mediating the general anesthetic effect, the reduction in the magnitude of the negative peak near the hydrophobic core, as with ethanol, and the lack of an effect on the peak near the membrane–water interface, in contrast with ethanol, indicates that the lateral pressure near the hydrophobic core may be a key in modulating ion channel function.

5. Reversibility of xenon effects

After equilibrium was reached at both 3 and 10 bar in the DSC experiments, a final set of measurements was taken to determine T_m after venting xenon from the system (see Fig. 4B and C and Table 1). Within an hour of xenon being removed from the system, the DEPC $T_{\beta\alpha}$ phase transition temperature was measured to be 11.4 ± 0.4 °C. While this value is within experimental error of T_m for pure DEPC liposomes prior to charging within xenon, it is likely that T_m is, in fact, slightly lower after venting xenon due to the residual amount of xenon in the system (a longer wait time after venting xenon would probably return the T_m to its original value of 11.8 °C). This rapid increase in T_m upon removal of xenon from the system indicates that the effects of xenon on T_m, and thus the fluidity, which are closely related, of lipid membranes are reversible.

To confirm the reversibility of the effects of xenon on lipid membranes, MD simulations were performed using the final configurations of the 200–300 ns double bilayer runs as starting configurations. The simulation parameters and setup were the same as those discussed in the Materials and methods section. In these simulations, xenon was manually removed from the aqueous phase but allowed to remain inside the bilayer and simulations were then run until a new equilibrium was reached, determined by monitoring the distribution of xenon in the bilayer and aqueous phase. Xenon was then removed from the aqueous phase again, and the simulations repeated. This process was done successively and the changes in bilayer properties were analyzed. Fig. S8 in the Supporting material shows the distribution of xenon between the bilayer and the aqueous phase for a xenon removal simulation. As expected based on the reversibility of the effects of xenon on liposome phase transition temperatures and in clinical usage, the xenon partitioned out of the bilayer, coming to a new equilibrium between the bilayer and the aqueous phase. As this repartitioning occurs, the properties of the lipid bilayer return toward their original values.

5.1. Discussion and conclusions

The combined results of the MD simulations and the DSC measurements provide a complex picture of the interactions between xenon and lipid membranes and the implications for membrane properties. It is clear that xenon, as with other small molecules [53,56,54,61,45], induces substantial structural changes in lipid membranes. The increase in area per lipid in the presence of xenon shown by the MD simulations indicates a concomitant increase in membrane fluidity. The substantial reduction in liposome phase transition temperature in the presence of xenon also indicates an increase in membrane fluidity and in bilayer surface area, consistent with the increase in area per lipid found in the MD simulations. Furthermore, as shown in Fig. 4A and Table 1, the T_m heat flow peaks shorten and widen as xenon permeates into the liposomes, suggesting a more inhomogeneous environment while the liposomes transition from the gel to the liquid–crystalline phase. As shown in Table 1, the phase transition temperature range increases by as much as 600% at a xenon pressure of 10 bar and, even at a relatively low xenon pressure of 3 bar, the presence of xenon still induces substantial widening of the phase transition region. This widening of the phase transition region has been shown for a variety of other small molecules [88], including several serotonin receptor agonists [89] and the anesthetics methoxyflurane [90], halothane, and enflurane [91]. We propose that the widening of the phase transition region induced by xenon is the result of an increase in the membrane surface area. The increased spacing between lipid head groups disrupts the continuum of the bilayer, broadening the phase transition, which is known to be a highly cooperative process [92,93].

A similar decrease in the membrane phase transition temperature has been shown experimentally for several other anesthetic agents. Trudell et al. [90] showed that clinical concentrations of methoxyflurane decreased the gel–liquid crystalline phase transition of mixed DPPC–DMPC bilayers. Similar results were reported by Mountcastle et al. [91] for halothane and enflurane with multilamellar DPPC liposomes. It is important to note, however, that not all small molecules induce changes in membrane phase transition temperature. Cater et al. found small to negligible effects of a variety of drugs, including morphine, on lipid phase transition temperatures [94].

As mentioned previously, the area per lipid in the bilayers increases significantly despite small increases in the order parameter of the lipid acyl chains (which was also reported by Stimson et al. [69]), a change normally associated with increased lipid packing and decreased bilayer surface area. The increase in surface area and membrane fluidity are confirmed by the DSC results. Furthermore, a simulation designed to assess the impact of the observed bilayer swelling on tail order parameter showed a substantial decrease in order parameter when the membrane swelled, independent of the other effects of xenon (see Fig. S9 in the Supporting material for additional information). Thus, we propose that the increased order parameter found in the simulation results represents a net local increase in ordering of the lipid acyl chains in the region between the *cis* double bonds and the terminal carbons, partly accounting for the observed increase in bilayer thickness. The increase in membrane fluidity associated with the increase in surface area occurs partly due to depression of the $L_{\beta\alpha}$ phase transition temperature, which is not well captured by the DOPC model used in the simulations. The significant number of xenon atoms present in the hydrophobic core of the bilayer exert steric-like effects on the surrounding acyl chains, forcing an increase in order and straightening of the tails but simultaneously inducing an increase in the lipid head group spacing. Using electron paramagnetic resonance techniques, Chin et al. [95] demonstrated that high pressure gases, including xenon, induced two effects in spin-labeled phospholipid bilayers: 1) initially, ordering in the bilayer increased, decreasing molecular motion in the plane of the bilayer, in a manner related to the increase in pressure; 2) on longer time scales, membrane fluidity was found to increase in a manner roughly corresponding to the lipid solubility of the gas. Thus, we propose that the accumulation of xenon in the bilayer decreases the lipid occupied volume within the membrane as a result of membrane swelling while simultaneously inducing net local ordering effects in a small region of the bilayer tails.

These results have substantial and significant implications for the potential of membrane-exerted effects on integral membrane proteins induced by xenon. The decrease in phase transition temperature caused by xenon is consistent with Heimburg's hypothesis of lipid

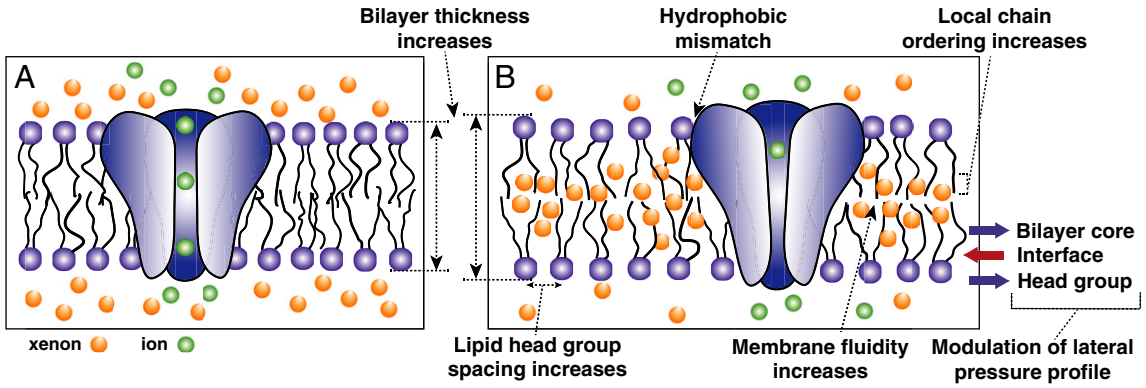

Fig. 6. Schematic representation of major changes in bilayer properties induced by xenon and hypothesized impacts on an ion-gated channel. (A) Lipid bilayer and ion channel prior to permeation of xenon. In the absence of xenon, the channel is in an open conformation, allowing the flux of ions. (B) Changes in bilayer properties when accommodating xenon and hypothesized membrane-mediated effects on the ion-gated channel. Ion flux through the channel is significantly reduced or completely stopped. Purple circles are lipid head groups, black lines are lipid tails, orange circles are xenon atoms, and green circles are ions.

membrane-induced anesthesia due to melting point depression by volatile anesthetics [47–49]. However, Heimburg's hypothesis has a number of flaws. Most significantly, while changes in temperature have been shown to induce substantial changes in lipid membrane fluidity, changes in temperature do not induce an anesthetic state and, as is acknowledged by Heimburg, application of anesthesia at temperatures substantially different than 310 K does not substantially change anesthetic potency. Thus, changes in membrane fluidity do not appear to be the main mechanism by which general anesthesia is induced. However, increases in membrane fluidity do affect the localization of membrane proteins, which has been implicated as mediating a number of cellular processes [96].

The thermodynamic and biophysical structural changes induced by xenon also alter the bilayer lateral pressure profile in the region of the bilayer head groups (see Fig. 5), consistent with Cantor's hypotheses on lipid membrane-induced anesthesia through modulation of the bilayer lateral pressure profile [42] and previous simulation results with ethanol [45]. The modulation of the membrane lateral pressure profile by xenon provides a mechanistic hypothesis for anesthetic action with xenon. This hypothesis accounts for, and indeed predicts, the violations of the Meyer–Overton correlation that have commonly been used as evidence against an indirect, lipid-bilayer mediated mechanism of general anesthesia [97].

However, a number of questions remain unresolved for Cantor's hypothesis. Indeed, the mechanism by which changes in lateral pressure profile would induce changes in transmembrane proteins must be further explored. An analysis by Phillips et al. [36] indicates that membrane-deformation free energy can potentially compete with the driving force for channel gating, thereby influencing the protein conformation. Thus, they conclude that, while the manner in which a specific protein interacts with a lipid membrane is highly specific, it is reasonable to expect that membrane proteins that alter their footprint within the membrane during a conformational change will be dependent on the structure of the membrane. However, specific protein targets for a lipid membrane-mediated mechanism of general anesthetic action have not been proposed so this mechanism remains speculative. Furthermore, as of yet, Cantor's lateral pressure profile hypothesis does not account for the fact that some general anesthetic agents, such as isoflurane [98,99], are chiral molecules, with different enantiomers exhibiting different anesthetic potencies. While chiral molecules do exist in many membranes, no lipid membrane-mediated mechanism accounting for the observed stereospecificity has been proposed [42]. Indeed, research by Dickinson et al. [100], among others, has indicated that it is not likely that chiral molecules in lipid membranes play a role in this stereospecificity. This argument does not apply to xenon as xenon is not a chiral molecule at physiological conditions but does limit the general applicability of the lateral pressure profile hypothesis in its current form.

The significant changes in lipid bilayer properties induced by xenon and the hypothesized effects on a gated ion channel are schematically summarized in Fig. 6. As illustrated, we suggest that gated ion channel function is indirectly impacted by the accumulated xenon in the membrane, which induces conformational changes in the ion channel, resulting in an altered flux of ions through the channel. The depression of the phase transition temperature, modulation of lateral forces on the channel, and inducement of hydrophobic mismatch due to membrane swelling each provide mechanisms for indirect action on ion channel conformation and function. Additionally, results of the calorimetry measurements and a set of MD simulations designed to test the reversibility of xenon's effects on lipid membranes are consistent with the clinical reversibility of the effects of general anesthesia. None of these findings preclude the possibility that general anesthetic agents, including xenon, interact directly with proteins to induce the effects of general anesthesia. Indeed, given the large body of evidence, it is likely that direct protein interactions are involved in mediation of the general anesthetic effect. However, our results suggest that a lipid bilayer-mediated mechanism may also play a role in mediating some or all of the effects of general anesthesia induced by xenon.

Acknowledgements

The authors thank Prof. Tsutomu Uchida (Hokkaido University, Japan) for his collaboration on this research, Prof. David Wu (Colorado School of Mines) for his comments and ideas, the Golden Energy Computing Organization (GECO) for providing computing resources, and the CSM Center for Hydrate Research for the use of the DSC. This work was partially funded by NSF grant CBET-0828649. A.K.S. acknowledges the support of DuPont for a DuPont Young Professor Award. Finally, we thank the reviewers for their thorough and insightful comments in the review of this manuscript.

Appendix A. Supplementary data

Supplementary data to this article can be found online at http://dx.doi.org/10.1016/j.bbamem.2013.01.016.

References

[1] B. Urban, Modern Anesthetics, J. Schüttler, H. Schwilden (Eds.), Spinger-Verlag, Berlin, 2008.
[2] The Joint Commission, Preventing, and managing the impact of, anesthesia awareness, Sentinel Event Alert 32 (2004) 1–3.
[3] H. Meyer, Zur theorie der alkoholnarkose, Naunyn-Schmiedebergs Arch. Pharmakol. 42 (1899) 109–118.
[4] C. Overton, Studien über die Narkose: Zugleich ein Beitrag zur Allgemeinen Pharmakologie, Verlag von Gustav Fischer, Jena, 1901.

[5] N.P. Franks, W.R. Lieb, Do general anaesthetics act by competitive binding to specific receptors? Nature 310 (1984) 599–601.
[6] P. Barash, B. Cullen, R. Stoelting, M. Stock, Handbook of Clinical Anesthesia, Lippincott, Williams, & Wilkins, Philadelphia, 2009.
[7] B. Urban, M. Bleckwenn, M. Barann, Interactions of anesthetics with their targets: non-specific, specific or both? Pharmacol. Ther. 111 (2006) 729–770.
[8] N. Franks, Molecular targets underlying general anaesthesia, Br. J. Pharmacol. 147 (2006) S72–S81.
[9] A. Lugli, C. Yost, C. Kindler, Anaesthetic mechanisms: update on the challenge of unravelling the mystery of anaesthesia, Eur. J. Anaesthesiol. 26 (2009) 807–820.
[10] S. Cullen, E. Gross, The anesthetic properties of xenon in animals and human beings, with additional observations on krypton, Science 113 (1951) 580–582.
[11] R. Sanders, N. Franks, M. Maze, Xenon: no stranger to anaesthesia, Br. J. Anaesth. 91 (2003) 709–717.
[12] A.R. Ravishankara, J.S. Daniel, R.W. Portmann, Nitrous oxide (N_2O): the dominant ozone-depleting substance emitted in the 21st century, Science 326 (2009) 123–125.
[13] T. Goto, K. Suwa, S. Uezono, F. Ichinose, M. Uchiyama, S. Morita, The blood–gas partition coefficient of xenon may be lower than generally accepted, Br. J. Anaesth. 80 (1998) 255–256.
[14] S. Wilhelm, D. Ma, M. Maze, N.P. Franks, Effects of xenon on in vitro and in vivo models of neuronal injury, Anesthesiology 96 (2002) 1485–1491.
[15] D. Ma, S. Wilhelm, M. Maze, N.P. Franks, Neuroprotective and neurotoxic properties of the 'inert' gas, xenon, Br. J. Anaesth. 89 (2002) 739–746.
[16] B. Lachmann, S. Armbruster, W. Schairer, M. Landstra, A. Trouwborst, G.J.V. Daal, A. Kusuma, W. Erdmann, Safety and efficacy of xenon in routine use as an inhalational anaesthetic, Lancet 335 (1990) 1413–1415.
[17] P. Harris, R. Barnes, The uses of helium and xenon in current clinical practice, Anesthesia 63 (2008) 284–293.
[18] A. Brücken, M. Coburn, S. Rex, R. Rossaint, M. Fries, Current developments in xenon research. Importance for anesthesia and intensive care medicine, Anaesthesist 59 (2010) 883–895.
[19] N. Franks, R. Dickinson, S. de Sousa, A. Hall, W. Lieb, How does xenon produce anaesthesia? Nature 396 (1998) 324.
[20] S.L. de Sousa, R. Dickinson, W.R. Lieb, N.P. Franks, Contrasting synaptic actions of the inhalational general anesthetics isoflurane and xenon, Anesthesiology 92 (2000) 1055–1066.
[21] E. Salmi, R. Laitio, S. Aalto, A. Maksimow, J. Långsjö, K. Kaisti, R. Aantaa, V. Oikonen, L. Metsähonkala, K. Någren, E. Korpi, H. Scheinin, Xenon does not affect gamma-aminobutyric acid type A receptor binding in humans, Anesth. Analg. 106 (2008) 129–134.
[22] T. Yamakura, R.A. Harris, Effects of gaseous anesthetics nitrous oxide and xenon on ligand-gated ion channels. comparison with isoflurane and ethanol, Anesthesiology 93 (2000) 1095–1101.
[23] J. Ogata, M. Shiraishi, T. Namba, C. Smothers, J. Woodward, R. Harris, Effects of anesthetics on mutant N-methyl-D-aspartate receptors expressed in *Xenopus* oocytes, J. Pharmacol. Exp. Ther. 318 (2006) 434–443.
[24] R. Dickinson, B. Peterson, P. Banks, C. Simillis, J. Martin, C. Valenzuela, M. Maze, N. Franks, Competitive inhibition at the glycine site of the N-methyl-D-aspartate receptor by the anesthetics xenon and isoflurane: evidence from molecular modeling and electrophysiology, Anesthesiology 107 (2007) 756–767.
[25] L. Liu, Y. Xu, P. Tang, Mechanistic insights into xenon inhibition of NMDA receptors from MD simulations, J. Phys. Chem. B 114 (2010) 9010–9016.
[26] P. Nagele, L. Metz, M. Crowder, Xenon acts by inhibition of non-N-methyl-D-aspartate receptor-mediated glutamatergic neurotransmission in *Caenorhabditis elegans*, Anesthesiology 103 (2005) 508–513.
[27] E. Eger, D. Raines, S. Shafer, H. Hemmings, J. Sonner, Is a new paradigm needed to explain how inhaled anesthetics produce immobility? Anesth. Analg. 107 (2008) 832–848.
[28] S. Rex, W. Schaefer, P. Meyer, R. Rossaint, C. Boy, K. Setani, U. Büll, J. Baumert, Positron emission tomography study of regional cerebral metabolism during general anesthesia with xenon in humans, Anesthesiology 105 (2006) 936–943.
[29] R. Laitio, J. Långsjö, S. Aalto, K. Kaisti, E. Salmi, A. Maksimow, R. Aantaa, V. Oikonen, T. Viljanen, R. Parkkola, H. Scheinin, The effects of xenon anesthesia on the relationship between cerebral glucose metabolism and blood flow in healthy subjects: a positron emission tomography study, Anesth. Analg. 108 (2009) 593–600.
[30] M. Gruss, T.J. Bushell, D.P. Bright, W.R. Lieb, A. Mathie, N.P. Franks, Two-pore-domain K+ channels are a novel target for the anesthetic gases xenon, nitrous oxide, and cyclopropane, Mol. Pharmacol. 65 (2004) 443–452.
[31] D. Pang, C. Robledo, D. Carr, T. Gent, A. Vyssotski, A. Caley, A.W.W. Zecharia, S. Brickley, N. Franks, An unexpected role for TASK-3 potassium channels in network oscillations with implications for sleep mechanisms and anesthetic action, Proc. Natl. Acad. Sci. U.S.A. 106 (2009) 17546–17551.
[32] R. Lazarenko, S. Willcox, S. Shu, A. Berg, J. Vesna, E. Talley, X. Chen, D. Bayliss, Motoneuronal task channels contribute to immobilizing effects of inhalational general anesthetics, J. Neurosci. 30 (2010) 7691–7704.
[33] M. Jensen, O. Mouritsen, Lipids do influence protein function — the hydrophobic matching hypothesis revisited, Biochim. Biophys. Acta 1666 (2004) 205–226.
[34] O. Andersen, R. Koeppe, Bilayer thickness and membrane protein function: an energetic perspective, Annu. Rev. Biophys. Bioeng. 36 (2007) 107–130.
[35] D. Marsh, Protein modulation of lipids, and vice-versa, in membranes, Biochim. Biophys. Acta 1778 (2008) 1545–1575.
[36] R. Phillips, T. Ursell, P. Wiggins, P. Sens, Emerging roles for lipids in shaping membrane–protein function, Nature 459 (2009) 379–385.
[37] D. Schmidt, R. MacKinnon, Voltage-dependent K+ channel gating and voltage sensor toxin sensitivity depend on the mechanical state of the lipid membrane, Proc. Natl. Acad. Sci. U.S.A. 105 (2008) 19276–19281.
[38] B. Martinac, O. Hamill, Gramicidin A channels switch between stretch activation and stretch inactivation depending on bilayer thickness, Proc. Natl. Acad. Sci. U.S.A. 99 (2002) 4308–4312.
[39] J. Lundbæk, R. Koeppe, O. Andersen, Amphiphile regulation of ion channel function by changes in the bilayer spring constant, Proc. Natl. Acad. Sci. U.S.A. 107 (2010) 15427–15430.
[40] J. Lundbæk, Lipid bilayer-mediated regulation of ion channel function by amphiphilic drugs, J. Gen. Physiol. 131 (2008) 421–429.
[41] R. Søgaard, T. Werge, C. Bertelsen, C. Lundbye, K. Madsen, C. Nielsen, J. Lundbaek, GABA(A) receptor function is regulated by lipid bilayer elasticity, Biochemistry 45 (2006) 13118–13129.
[42] R.S. Cantor, The lateral pressure profile in membranes: a physical mechanism of general anesthesia, Biochemistry 36 (1997) 2339–2344.
[43] Y. Suezaki, A. Petrov, I. Ueda, Theoretical model of anesthetic action upon ion channels mediated by lipid membrane, Int. Congr. Ser. 1283 (2005) 227–230.
[44] D. Marsh, Lateral pressure profile, spontaneous curvature frustration, and the incorporation and conformation of proteins in membranes, Biophys. J. 93 (2007) 3884–3899.
[45] E. Terama, O. Ollila, E. Salonen, A. Rowat, C. Trandum, P. Westh, M. Patra, M. Karttunen, I. Vattulainen, Influence of ethanol on lipid membranes: from lateral pressure profiles to dynamics and partitioning, J. Phys. Chem. B 112 (2008) 4131–4139.
[46] B. Griepernau, R. Böckmann, The influence of 1-alkanols and external pressure on the lateral pressure profiles of lipid bilayers, Biophys. J. 95 (2008) 5766–5778.
[47] T. Heimburg, A. Jackson, On soliton propagation in biomembranes and nerves, Proc. Natl. Acad. Sci. U.S.A. 102 (2005) 9790–9795.
[48] T. Heimburg, A. Jackson, The thermodynamics of general anesthesia, Biophys. J. 92 (2007) 3159–3165.
[49] T. Heimburg, A. Jackson, On the action potential as a propagating density pulse and the role of anesthetics, Biophys. Rev. Lett. 2 (2007) 1–22.
[50] S. Singer, G. Nicolson, The fluid mosaic model of the structure of cell membranes, Science 175 (1972) 720–731.
[51] R. Cherry, Protein mobility in membranes, FEBS Lett. 55 (1975) 1–7.
[52] R. Venable, Y. Zhang, B. Hardy, R. Pastor, Molecular dynamics simulations of a lipid bilayer and of hexadecane: an investigation of membrane fluidity, Science 262 (1993) 223–226.
[53] S. Marrink, H. Berendsen, Permeation process of small molecules across lipid membranes studied by molecular dynamics simulations, J. Phys. Chem. 100 (1996) 16729–16738.
[54] D. Bemporad, J. Essex, C. Luttmann, Permeation of small molecules through a lipid bilayer: a computer simulation study, J. Phys. Chem. B 108 (2004) 4875–4884.
[55] J. MacCallum, D. Tieleman, Computer simulation of the distribution of hexane in a lipid bilayer: spatially resolved free energy, entropy, and enthalpy profiles, J. Am. Chem. Soc. 128 (2006) 125–130.
[56] A. Sum, R. Faller, J. Pablo, Molecular simulation study of phospholipid bilayers and insights of the interactions with disaccharides, Biophys. J. 85 (2003) 2830–2844.
[57] B. Lee, R. Faller, A. Sum, I. Vattulainen, M. Patra, M. Karttunen, Structural effects of small molecules on phospholipid bilayers investigated by molecular simulations, Fluid Phase Equilib. 225 (2004) 63–68.
[58] C. Pereira, R. Lins, I. Chandrasekhar, L. Freitas, P. Hünenberger, Interaction of the disaccharide trehalose with a phospholipid bilayer: a molecular dynamics study, Biophys. J. 86 (2004) 2273–2285.
[59] S. Leekumjorn, A. Sum, Molecular dynamics study on the stabilization of dehydrated lipid bilayers with glucose and trehalose, J. Phys. Chem. B 112 (2008) 10732–10740.
[60] S. Feller, C. Brown, D. Nizza, K. Gawrisch, Nuclear overhauser enhancement spectroscopy cross-relaxation rates and ethanol distribution across membranes, Biophys. J. 82 (2002) 1396–1404.
[61] M. Patra, E. Salonen, E. Terama, I. Vattulainen, R. Faller, B. Lee, J. Holopainen, M. Karttunen, Under the influence of alcohol: the effect of ethanol and methanol on lipid bilayers, Biophys. J. 90 (2006) 1121–1135.
[62] M. Kaye, K. Schmalzl, V.C. Nibali, M. Tarek, M. Rheinstädter, Ethanol enhances collective dynamics of lipid membranes, Phys. Rev. E 83 (2011), (05097–1–4).
[63] T. Sirk, E. Brown, A. Sum, M. Friedman, Molecular dynamics study on the biophysical interactions of seven green tea catechins with lipid bilayers of cell membranes, J. Agric. Food Chem. 56 (2008) 7750–7758.
[64] T. Sirk, E. Brown, M. Friedman, A. Sum, Molecular binding of catechins to biomembranes: relationship to biological activity, J. Agric. Food Chem. 57 (2009) 6720–6728.
[65] M. Pickholz, L. Saiz, M. Klein, Concentration effects of volatile anesthetics on the properties of model membranes: a coarse-grain approach, Biophys. J. 88 (2005) 1524–1534.
[66] L. Koubi, M. Tarek, M. Klein, D. Scharf, Distribution of halothane in a dipalmitoylphosphatidylcholine bilayer from molecular dynamics calculations, Biophys. J. 78 (2000) 800–811.
[67] P. Tang, Y. Xu, Large-scale molecular dynamics simulations of general anesthetic effects on the ion channel in the fully hydrated membrane: the implication of molecular mechanisms of general anesthesia, Proc. Natl. Acad. Sci. U.S.A. 99 (2002) 16035–16040.
[68] S. Vemparala, L. Saiz, R. Eckenhoff, M. Klein, Partitioning of anesthetics into a lipid bilayer and their interaction with membrane-bound peptide bundles, Biophys. J. 91 (2006) 2815–2825.
[69] L. Stimson, I. Vattulainen, T. Róg, M. Karttunen, Exploring the effect of xenon on biomembranes, Cell. Mol. Biol. Lett. 10 (2005) 563–569.

[70] E. Yamamoto, T. Akimoto, H. Shimizu, Y. Hirano, M. Yasui, K. Yasuoka, Diffusive nature of xenon anesthetic changes properties of a lipid bilayer: molecular dynamics simulations, J. Phys. Chem. B 116 (2012) 8989–8995.
[71] K.M. Tu, N. Matubayasi, K.K. Liang, I.T. Todorov, S.L. Chan, P.-L. Chau, A possible molecular mechanism for the pressure reversal of general anaesthetics: aggregation of halothane in POPC bilayers at high pressure, Chem. Phys. Lett. 543 (2012) 148–154.
[72] M. Darvas, P. Hoang, S. Picaud, M. Sega, P. Jedlovszky, Anesthetic molecules embedded in a lipid membrane: a computer simulation study, Phys. Chem. Chem. Phys. 14 (2012) 12956–12969.
[73] S.C. Cullen, E.I. Eger, B.F. Cullen, P. Gregory, Observations on the anesthetic effect of the combination of xenon and halothane, Anesthesiology 31 (1969) 305–309.
[74] O. Berger, O. Edholm, F. Jähnig, Molecular dynamics simulations of a fluid bilayer of dipalmitoylphosphatidylcholine at full hydration, constant pressure, and constant temperature, Biophys. J. 72 (1997) 2002–2013.
[75] H. Berendsen, J. Postma, W. van Gunsteren, J. Hermans, Intermolecular Forces, Reidel, Dordrecht, 1981.
[76] J. Hirschfelder, C. Curtiss, R. Bird, Molecular Theory of Gases and Liquids, John Wiley & Sons, Inc., New York, 1954.
[77] B. Hess, C. Kutzner, D. van der Spoel, E. Lindahl, GROMACS 4: algorithms for highly efficient, load-balanced, and scalable molecular simulation, J. Chem. Theory Comput. 4 (2008) 435–447.
[78] H. Berendsen, J. Postma, W. van Gunsteren, J. Haak, Molecular dynamics with coupling to an external bath, J. Chem. Phys. 81 (1984) 3684–3690.
[79] J. Silvius, Thermotropic Phase Transitions of Pure Lipids in Model Membranes and Their Modifications by Membrane Proteins, John Wiley & Sons, Inc., New York, 1982.
[80] T. Darden, D. York, L. Pedersen, Particle mesh Ewald: an nlog(n) method for Ewald sums in large systems, J. Chem. Phys. 98 (1993) 10089–10092.
[81] U. Essmann, L. Perera, M. Berkowitz, T. Darden, H. Lee, L. Pedersen, A smooth particle mesh Ewald method, J. Chem. Phys. 103 (1995) 8577–8593.
[82] B. Hess, H. Bekker, H.J.C. Berendsen, J.G.E.M. Fraaije, LINCS: a linear constraint solver for molecular simulations, J. Comput. Chem. 18 (1997) 1463–1472.
[83] D.P. Tieleman, S.J. Marrink, H.J. Berendsen, A computer perspective of membranes: molecular dynamics studies of lipid bilayer systems, Biochim. Biophys. Acta 1331 (1997) 235–270.
[84] M. Alwarawrah, J. Dai, J. Huang, A molecular view of the cholesterol condensing effect in DOPC lipid bilayers, J. Phys. Chem. B 114 (2010) 7516–7523.
[85] R. Booker, C. Koh, E. Sloan, A. Sum, E. Shalaev, S. Singh, Xenon hydrate dissociation measurements with model protein systems, J. Phys. Chem. B 115 (2011) 10270–10276.
[86] O.H. Ollila, H.J. Risselada, M. Louhivuori, E. Lindahl, I. Vattulainen, S.J. Marrink, 3D pressure field in lipid membranes and membrane–protein complexes, Phys. Rev. Lett. 102 (2009) 1–4.
[87] O.H. Ollila, M. Hyvonen, I. Vattulainen, Polyunsaturation in lipid membranes: dynamic properties and lateral pressure profiles, J. Phys. Chem. B 111 (2007) 3139–3150.
[88] M. Jain, N. Wu, Effect of small molecules on the dipalmitoyl lecithin liposomal bilayer: III. Phase transition in lipid bilayer, J. Membr. Biol. 34 (1977) 157–201.
[89] R. Batchelor, C.J. Windle, S. Buchoux, M. Lorch, Cholesterol and lipid phases influence the interactions between serotonin receptor agonists and lipid bilayers, J. Biol. Chem. 285 (2010) 41402–41411.
[90] J.R. Trudell, D.G. Payan, J.H. Chin, E.N. Cohen, The antagonistic effect of an inhalation anesthetic and high pressure on the phase diagram of mixed dipalmitoyldimyristoylphosphatidylcholine bilayers, Proc. Natl. Acad. Sci. U.S.A. 72 (1975) 210–213.
[91] D.B. Mountcastle, R.L. Biltonen, M.J. Halsey, Effect of anesthetics and pressure on the thermotropic behavior of multilamellar dipalmitoylphosphatidylcholine liposomes, Proc. Natl. Acad. Sci. U.S.A. 75 (1978) 4906–4910.
[92] J. Nagle, Theory of lipid monolayer and bilayer phase transitions: effect of headgroup interactions, J. Membr. Biol. 27 (1976) 233–250.
[93] D. Marsh, A. Watts, P.F. Knowles, Cooperativity of the phase transition in single- and multibilayer lipid vesicles, Biochim. Biophys. Acta 465 (1977) 500–514.
[94] B.R. Cater, D. Chapman, S.M. Hawes, J. Saville, Lipid phase transitions and drug interactions, Biochim. Biophys. Acta 363 (1974) 54–69.
[95] J.H. Chin, J.R. Trudell, E.N. Cohen, The compression-ordering and solubility-disordering effects of high pressure gases on phospholipid bilayers, Life Sci. 18 (1976) 489–497.
[96] D. Lingwood, K. Simons, Lipid rafts as a membrane-organizing principle, Science 327 (2010) 46–50.
[97] R.S. Cantor, Breaking the Meyer–Overton rule: predicted effects of varying stiffness and interfacial activity on the intrinsic potency of anesthetics, Biophys. J. 80 (2001) 2284–2297.
[98] B. Harris, E. Moody, P. Skolnick, Isoflurane anesthesia is stereoselective, Eur. J. Anaesthesiol. 217 (1992) 215–216.
[99] G.S. Lysko, J.L. Robinson, R. Castro, R.A. Ferrone, The stereospecific effects of isoflurane isomers in vivo, Eur. J. Anaesthesiol. 263 (1994) 25–29.
[100] R. Dickinson, N.P. Franks, W.R. Lieb, Can the stereoselective effects of the anesthetic isoflurane be accounted for by lipid solubility? Biophys. J. 66 (1994) 2019–2023.